Parametric study of a wave energy converter (Searaser) for Caspian Sea

Babajani, Aliakbar ; Jafari, Mohammad ; Hafezisefat, Parinaz ; Hosseini, Seyed Mojtaba Mir; Rezaniakolaei, Alireza; Rosendahl, Lasse Aistrup

Published in:
Energy Procedia

DOI (link to publication from Publisher):
10.1016/j.egypro.2018.07.101

Publication date:
2018

Document Version
Publisher's PDF, also known as Version of record

Available online at www.sciencedirect.com

ScienceDirect

Energy Procedia 147 (2018) 334–342

Energy Procedia

www.elsevier.com/locate/procedia

International Scientific Conference "Environmental and Climate Technologies", CONECT 2018

Parametric study of a wave energy converter (Searaser) for Caspian Sea

Aliakbar Babajani[a], Mohammad Jafari[b]*, Parinaz Hafezisefat[c], Mojtaba Mirhosseini[d], Alireza Rezania[d], Lasse Rosendahl[d]

[a]*Department of Mechanical Engineering, Shahrekord University, Shahrekord, 53849-88176, Iran*
[b]*Department of Aerospace Engineering, Iowa State University, Ames, 50011, USA*
[c]*Department of Mechanical Engineering, Iowa State University, Ames, 50011, USA*
[d]*Department of Energy Technology, Aalborg University, Pontoppidanstraede 111, Aalborg East, 9220, Denmark*

Abstract

Over the past decades, different types of energy converters have been invented because wave energy is a renewable energy source with high potential for extraction of considerable clean energy. Many numerical and experimental tests have been conducted to calculate the power generation of ocean waves, and these tests have demonstrated the significance of this energy. In this paper, the hydrodynamic performance of a new energy converter called "Searaser" has been evaluated using numerical simulation to study different aspects of this energy converter. Since previous studies have found ocean wave energy converters excellent for implementation in the Caspian Sea, the aim of this study is to investigate its performance for that sea, so this study presents a numerical simulation of Searaser inside an experimental wave tank using commercial software *Flow*-3D. To model the motion of the energy converter, Reynolds Averaged Navier-Stokes was coupled with a volume-of-fluid (VOF) model to generate three-dimensional numerical linear propagating waves for solving the fluid field. Grid independency was also carried out to determine the best mesh numbers for the original simulations. Finally, the Searaser hydrodynamic performance was numerically calculated for different wave heights, and some of the most important parameters of point absorbers were captured, including output flow rate in different seasons, extractable wave power, and output power. Accordingly, the obtained results indicate that the output flow rate and the power generation are significantly increased by incremental changes in wave height, and using this type of converter device has potential for practical and profitable use in industrial applications.

* Corresponding author.
E-mail address: mjafari@iastate.edu

1876-6102
10.1016/j.egypro.2018.07.101

Keywords: renewable energy; Searaser; ocean wave energy converter (OWEC); fluid structure interaction (FSI); Caspian Sea

1. Introduction

Energy consumption is increasing every year because of population growth. Since sources of fossil fuels are limited and are not considered to be clean energy, many countries have decided to generate more power from renewable energy such as that from ocean waves. Wave energy offers several benefits in comparison with other renewable energies, e.g., it is widely available, predictable, and represents higher energy densities that could produce more power with lower cost. Since many numerical techniques have been used to evaluate performance of different engineering applications like turbomachinery [1–5] and heat transfer [6–10], and these methods have demonstrated good agreement between numerical and experimental result, a numerical approach has been employed in this paper to simulate the motion of a novel energy convertor called "Searaser" for use in the Caspian Sea [11].

So far, many numerical and experimental studies [12–15] of energy converters have been conducted, and some of them are briefly reviewed here. Generally, there are different types of wave-energy converter (WEC) systems, and WEC can be categorized into four groups: oscillating water column, overtopping device, attenuator, and point absorber [16]. Operation of the first type, the oscillating water column (OWC), is based on air compression and decompression. Recently, some theoretical optimization studies for spare buoys have been carried out [17, 18]. The best-known turbines for OWCs are Wells and Impulse turbines [19]. Falco et al. [20, 21] presented the comparison between a Wells turbine to a new bi-radial Impulse turbine. The second group, overtopping devices, utilize wave velocity for filling a reservoir located in a higher level than the ocean surface, then the water descends through low-head turbines to produce electricity. Some familiar examples of overtopping devices are the Wave Dragon [22], SSG [23] and the WaveCat [24]. The third group, attenuators, use floating buoys parallel to the wave direction connected to one another. Pelamis is a snake-like device that consists of cylindrical bodies connected together [25]. The last group, point absorbers, convert energy using buoys that capture the heaving motions of wave, the vertical motion of waves is used to compress gas or liquid that drives a power generator and produce electricity. Point absorbers can be further divided into single-body or multiple-body devices. Single-body point absorbers move through a fixed seabed and multiple-body devices generate electricity by motion of two bodies [26]. Recently, many researchers are interested in minimizing the energy consumption and cost [27–30], which can be done some financial calculation for point absorbers as well. Although many studies have been conducted on these devices, using numerical simulation to measure hydro-acoustic of energy converters is preferred to avoid dangers to ocean animals. So far, many studies have used numerical technique to calculate the noise for a variety of engineering applications [31–34].

In 2013, a new OWEC named "Searaser" was invented [35]. It consists of a cylinder attached to a piston, which is forced upwards by the buoyancy force since it is floating on the water surface when the ocean waves approach the device. Afterward, the gravity force of body overcomes other forces such as dynamic forces and wall friction after passing waves, and it causes to move buoy downward gradually (see Fig. 1). This device employs the periodic motion of waves to pump the ocean water to higher level (on-shore) in order to store it in large ponds and generate electricity with a turbine and generator on demand. Searaser has many notable advantages which some of them are mentioned here. It offers some exceptional benefits compared with similar types on the market:

- First, the price of components decreases because the components producing the electricity (turbine and generator) are separated from the Searasers, an advantage because generating electricity on the ocean surface requires special components to deal with corrosion;
- Second, electricity produced by Searaser is obviously considered to be clean energy since there are no climate gas emissions involved (at least not after construction and installation);
- As another benefit, it has a simpler design and uses cheaper components than other wave energy converters, making this invention somewhat special;

- Another advantage is that the output water from this device can be transferred to an area designated for offshore wind turbines and thereby help in creating a more effective area.

In this study, the performance of Searaser in a wave tank was studied by solving Navier-Stokes equations using a commercial computational fluid dynamics (CFD) software package (*Flow*-3D), appropriate for numerical modelling of WEC, to solve the governing equations. Following this, the performance of a Searaser with geometric dimensions based on the data extracted from the patent was numerically evaluated for varied wave heights. Ultimately, the results demonstrate that power generation obviously increases by incrementing increases in wave heights.

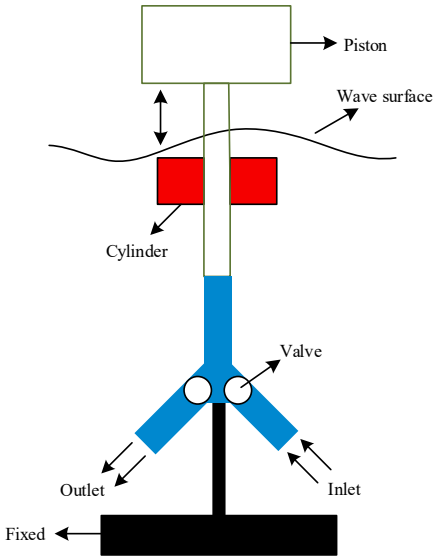

Fig. 1. Schematic of different components of a Searaser.

Nomenclature

$\vec{\omega}$	angular velocity, rad/s
$\overrightarrow{V_G}$	velocity of mass center, m/s
$\vec{F}$	total force, N
m	mass of the rigid body, kg
$\overrightarrow{T_G}$	total torque about G, N·m
[J]	moment of inertia tensor about G in a body proportional referenced system, kg·m^2
$\overrightarrow{F_a}$	gravitational force
$\overrightarrow{F_h}$	hydraulic force due to the pressure field and the wall shear forces on the moving body
$\overrightarrow{F_c}$	net control force of the network that can be used for controlling and confining the rigid body motion
$\overrightarrow{F_{nt}}$	non-inertial force when the rigid body moves in a non-inertial space system

ρ	fluid density (water in this case), kg/m^3
$\vec{u}$	velocity of fluid, m/s
V_f	volume fraction
A_f	area fractio
p	pressure, Pa
τ	viscous stress tensor, Pa
G	gravity, m/s^2
F	fluid fraction
A	outlet area of flow from the Searaser, m^2
Q	outlet volume flow rate, m^3/s
$\dot{P}$	output power, W
H_s	wave height, m
T	wave period, s
ρ	water density, kg/m^3
g	gravity, m/s^2
P	extractable power, W/m

2. Governing equations

Flow-3D uses a unique technique named *FAVOR* to describe geometric objects in a computational domain, which is based on the concept of area fraction (AF) and volume fraction (VF) in a rectangular structured mesh. The VF is defined as the ratio of open volume to the total volume in a cell whereas three AF's (AFR, AFB, AFT) are defined for three cell faces respectively in the direction of increasing cell-index as the ratio of the open area to the total area. This *FAVOR* technique works well with complex geometries by introducing the effects of AF and VF into the conservation equations of fluid flow. This technique has led to the successful development of a general moving object (GMO) capability which in principle permits the modelling of any type of rigid body motion (six degree of freedom, fixed axis and fixed point) on a fixed-mesh. This particular simulation is the application of this GMO model to a fixed axis dynamically coupled motion of WRASPA and Searaser. Solver calculates AF and VF at each time step, which describes object's motion through a fixed-rectangular mesh. Hydraulic, gravitational, and control forces and torques are calculated and equations of motion for the rigid body are solved explicitly for translational and rotational velocities of moving objects under a coupled motion.

2.1 Equations of movement (rigid body)

In general, each motion of a rigid body can be divided into translational and rotational movements. The velocity of each single moving point is equal to the optional base point velocity plus the velocity that is originated from the rotation of the body around the base point. For movement in 6 degrees of freedom, the general moving object (GMO) model considers the mass center of the body (G) as the base point. The equations for 6 degree of freedom movement are divided into two separate following equations [36]:

$$\vec{F} = m\frac{d\vec{V_G}}{dt} \tag{1}$$

$$\vec{T_G} = [J]\cdot\frac{d\vec{\omega}}{dt} + \vec{\omega}\cdot([J]\cdot\vec{\omega}) \tag{2}$$

Total force and total torque are calculated as the summation of some different components as follow:

$$\vec{F} = \vec{F}_g + \vec{F}_h + \vec{F}_c + \vec{F}_{nt} + \vec{F}_i \tag{3}$$

$$\overrightarrow{T_G} = \vec{T}_g + \vec{T}_h + \vec{T}_c + \vec{T}_{nt} \tag{4}$$

In this case there is no $\overrightarrow{F_{nt}}$, so $\overrightarrow{T_G}$, $\overrightarrow{T_g}$, $\overrightarrow{T_h}$, $\overrightarrow{T_c}$ and $\overrightarrow{T_{nt}}$ are the total torque, gravitational torque, hydraulic torque, control torque and non-inertial torque, respectively, around the mass center of the rigid body. The continuity and momentum equations for a moving body and the relative transport are given by:

$$\frac{V_f}{\rho}\frac{\partial \rho}{\partial t} + \frac{1}{\rho}\nabla \cdot (\rho \vec{u} A) = -\frac{\partial V_f}{\partial t} \tag{5}$$

$$\frac{\partial \vec{u}}{\partial t} + \frac{1}{V_f}(\vec{u}A_f \cdot \nabla \vec{u}) = -\frac{1}{\rho}[\nabla p + \nabla \cdot (\tau A_f)] + \vec{G} \tag{6}$$

$$\frac{\partial F}{\partial t} + \frac{1}{V_f}\nabla \cdot (F \vec{u} A_f) = -\frac{F}{V_f}\frac{\partial V_f}{\partial t} \tag{7}$$

For coupling of the GMO's motion, Eq. (1) and Eq. (2) should be solved at each time step, the situation of all the objects recorded, and the volume fraction updated using the *FAVOR* technique.

3. Grid independency

Grid examination is usually essential in choosing a sufficiently-sized grid, so four grids were generated with 298320, 504186, 723451, and 904450 cells (Block 1) to simulate a 3D Searaser experiencing a moving wave with a height of 1.25 m. The number of grid elements was increased in mesh blocks to improve the accuracy of the solution. In Fig. 2, the volume flow rate at the outlet was measured at various times, and when comparing the curves, it was obvious that the grid with 504186 cells was suitable for the present study, so this grid was chosen for all simulations in this study.

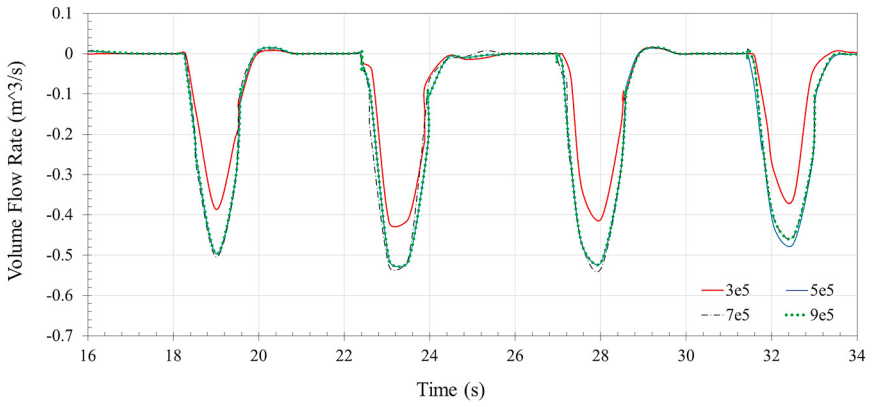

Fig. 2. Comparison of outlet volume flow rate for a wave amplitude 1.25 m.

In Table 1, run time is shown for different cell sizes for time average of 17.5 s.

Table 1. Run time for different mesh sizes.

Mesh	Total cells	Smallest cell size (Block 1), m	Run time for t_{avg} = 17.5 sec.
1	963210	0.006	1 day 7 hr
2	1516695	0.004	2 days 8 hr
3	1952904	0.002	3 days

4. Results and discussion

In this section the results of modelling Searaser is illustrated. In order for better understanding, pressure contour of Searaser in the wave tank was plotted in Fig. 3 for different times including 0 s, 42.5 s, 44 s and 45 s. Additionally, this figure indicates the movement of ocean wave, outlet and inlet valve at different times.

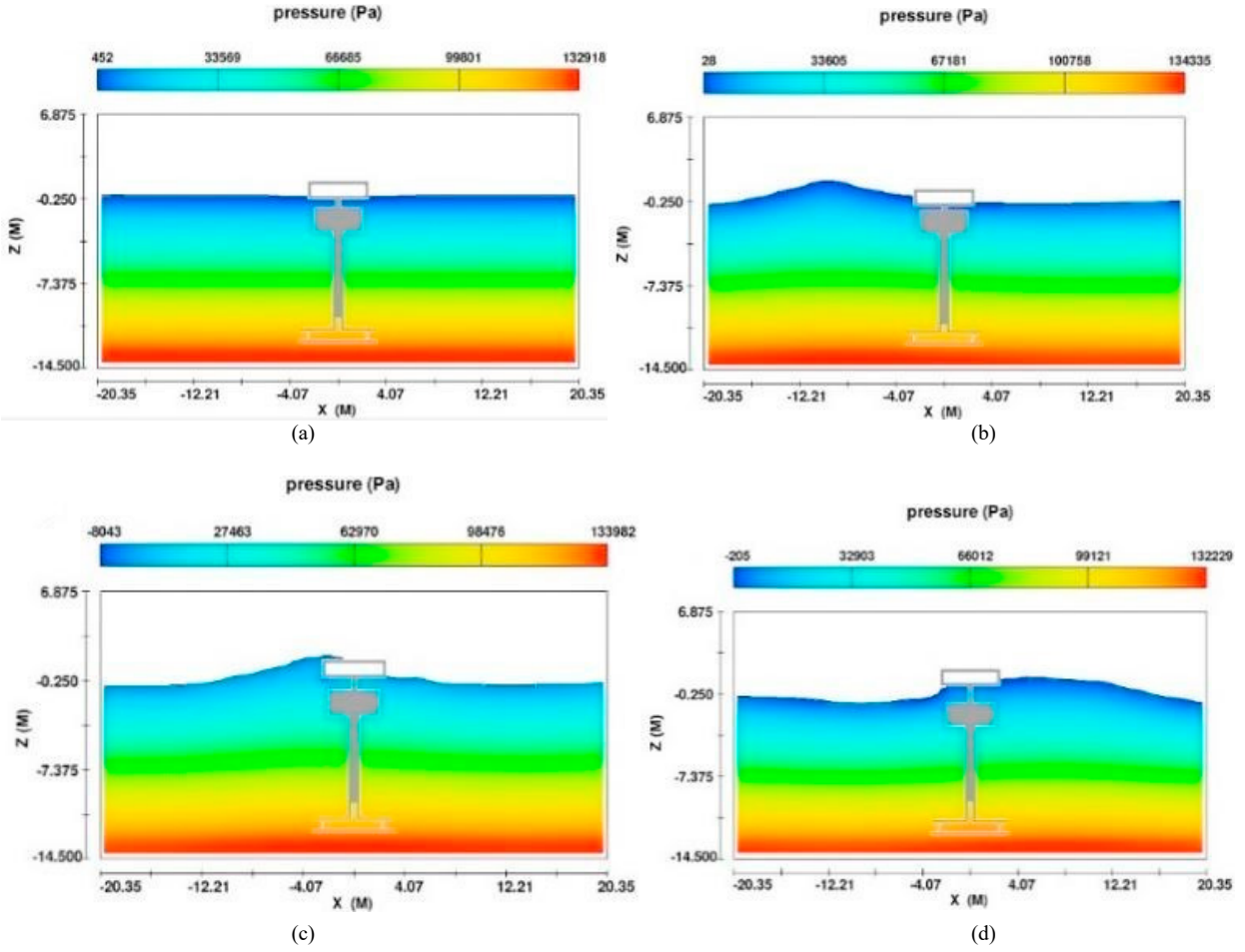

Fig. 3. Pressure contour of wave motion at different times: (a) 0 s; (b) 42.5 s; (c) 44 s; (d) 45 s.

In Fig. 4, based on Eq. (8), the output power of Searaser for four wave heights was calculated in different times:

$$\dot{P} = \frac{1}{2A^2}\rho Q^3 \tag{8}$$

As can be seen clearly in this figure, the output power is extremely dependent on the wave height. This plot shows that the device produces no output power in 4.5 s (wave period) because the upper buoy exhibits no any movement when there is no ocean wave. This cycle is repeated periodically for each wave height, obviously an undesirable result when the purpose is to produce electricity continuously.

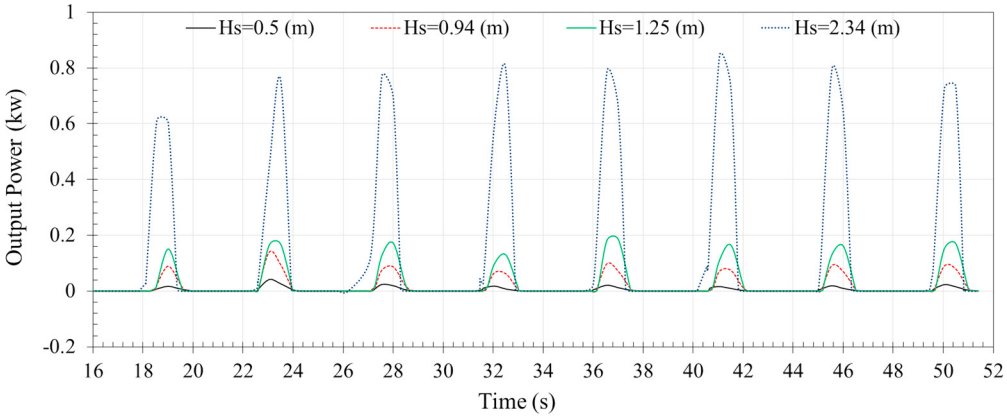

Fig. 4. Output power of Searaser for four wave heights.

The summary of wave height in Caspian Sea is reported in Table 3. The maximum output power from this device for different wave heights are listed in Table 4. This list shows that the maximum output power in winter and the minimum output power in summer are 0.8 kW and 0.02 kW, respectively. In comparison with other wave energy converters of this type, such as L10 and Upsala, while the output power of Searaser is lower [28], it has less manufacturing costs and can be replicated in large numbers for increasing output power at a chosen area. In Fig. 5, output power versus H_s is depicted, and its equation is similar to that of the extractable power [38] (Eq. (12)) since the power varies quadratically in both. Eq. (9) can be used [28].

$$P = \frac{1}{64\pi}\rho g^2 H_s^2 T \tag{9}$$

Table 2. Different wave heights for the south of Caspian Sea [39].

Season	Mean, m	95th, m
Summer	0.5	1.25
Winter	0.94	2.34

Table 3. Extractable and output power for Searaser.

Wave height, m	Maximum extractable power, kW/m	Maximum output power, kW
0.5	0.54	0.02
0.94	1.9	0.1
1.25	3.37	0.17
2.34	11.79	0.8

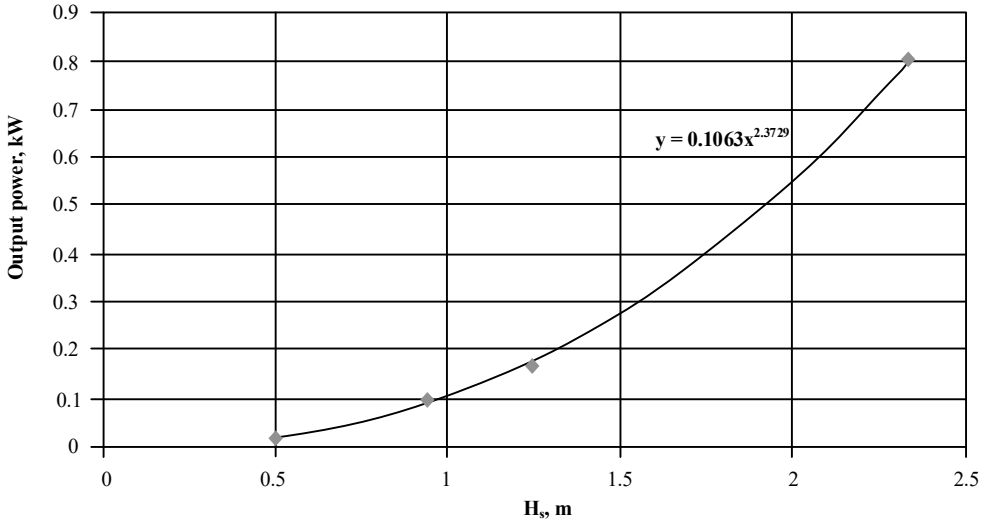

Fig. 5. Curve of output power versus H_s.

5. Conclusion

Recently, many studies have proven that ocean wave energy convertors offer the most appropriate systems for harvesting the Caspian Sea wave energy, so this study presents a numerical simulation of Searaser inside a wave tank using commercial flow software *Flow*-3D. To simulate this energy converter, Reynolds Averaged Navier-Stokes equations were coupled with a volume-of-fluid (VOF) model to generate 3D numerical linear propagating waves as well as to solve for fluid flow. The hydrodynamic performance of Searaser was numerically calculated for different Caspian Sea wave heights. Moreover, the most important parameters of point absorbers, including output flow rate in different seasons, extractable wave power, and output power, were captured. The results indicate that the output flow rate and the power generation increase significantly with increased increments of wave heights, and using this device has the potential to provide practical and profitable systems for industrial applications.

References

[1] Khaleghi H, Dehkordi MA, Tousi AM. Role of tip injection in desensitizing the compressor to the tip clearance size. Aerospace Science and Technology 2016;52:10–7.

[2] Mortazavi F, Palazzolo A. Prediction of Rotordynamic Performance of Smooth Stator-Grooved Rotor Liquid Annular Seals Utilizing Computational Fluid Dynamics. Journal of Vibration and Acoustics 2018;140(3):031002.

[3] Jafari MM, Atefi GA, Khalesi J. Advances in nonlinear stress analysis of a steam cooled gas turbine blade. Latin American applied research 2012;42(2):167–75.

[4] Mortazavi F, Palazzolo A. CFD-Based Prediction of Rotordynamic Performance of Smooth Stator-Grooved Rotor (SS-GR) Liquid Annular Seals. ASME Turbo Expo: Turbomachinery Technical Conference and Exposition, USA, North Carolina, June 26–30, 2017.

[5] Ghoreyshi SM, Schobeiri MT. Numerical Simulation of the Multistage Ultra-High Efficiency Gas Turbine Engine, UHEGT. ASME Turbo Expo: Turbomachinery Technical Conference and Exposition, USA, North Carolina, June 26–27, 2017.

[6] Hafezisefat P, Esfahany MN, Jafari M. An experimental and numerical study of heat transfer in jacketed vessels by SiO_2 nanofluid. Heat and Mass Transfer 2017;53(7):2395–405.

[7] Jafari MM, Atefi G, Khalesi J, Soleymani A. A new conjugate heat transfer method to analyse a 3D steam cooled gas turbine blade with temperature-dependent material properties. Proceedings of the Institution of Mechanical Engineers, Part C: Journal of Mechanical Engineering Science 2012;226(5):1309–20.

[8] Ramezani M, Legg MJ, Haghighat A, Li Z, Vigil RD, Olsen MG. Experimental investigation of the effect of ethyl alcohol surfactant on oxygen mass transfer and bubble size distribution in an air-water multiphase Taylor-Couette vortex bioreactor. Chemical Engineering Journal 2017;319:288–96.

[9] Haghighat AK, Roumi S, Madani N, Bahmanpour D, Olsen MG. An intelligent cooling system and control model for improved engine thermal management. Applied Thermal Engineering 2018;128:253–63.

[10] Rahbari I, Mortazavi F, Rahimian MH. High order numerical simulation of non-Fourier heat conduction: An application of numerical Laplace

transform inversion. International Communications in Heat and Mass Transfer 2014;51:51–8.
[11] Babajani AA, Jafari M, Sefat PH. Numerical investigation of distance effect between two Searasers for hydrodynamic performance. Alexandria Engineering Journal 2016;55(3):2257–68.
[12] Falcao AF, Henriques JC, Gato LM, Gomes RP. Air Turbine Choice and Optimization for Floating Oscillating-Water-Column Wave Energy Converter. Ocean Engineering 2014;75:148–56.
[13] Merigaud A, Ringwood JV. A Nonlinear Frequency-Domain Approach for Numerical Simulation of Wave Energy Converters. IEEE Transactions on Sustainable Energy 2018;9(1):86–94.
[14] Goodarzi M, Khalesi J. Experimental and Numerical Studies on Frequency and Damping of Liquid Oscillation in a Storage Tank. Aerospace Mechanics Journal 2012;7(426):25–34.
[15] Elhanafi A, Macfarlane G, Fleming A, Leong Z. Experimental and numerical investigations on the hydrodynamic performance of a floating–moored oscillating water column wave energy converter. Applied Energy 2017;205:369–90.
[16] Brekken T, von Jouanne A, Han HY. Ocean Wave Energy Overview and Research at Oregon State University. In Power Electronics and Machines in Wind Applications. PEMWA 2009;1 –7.
[17] Gomes RPF, Henriques JCC, Gato LMC, Falcao AFO. Hydrodynamic Optimization of an Axisymmetric Floating Oscillating Water Column for Wave Energy Conversion. Renewable Energy 2012;44:328–39.
[18] Falcao A.FO, Henriques JCC, Candido JJ. Dynamics and Optimization of the OWC Spar Buoy Wave Energy Converter. Renewable Energy 2012;48:369–81.
[19] Falcao AF, Henriques JC, Gato LM, Gomes RP. Air Turbine Choice and Optimization for Floating Oscillating-Water-Column Wave Energy Converter. Ocean Engineering 2014;75:148–56.
[20] Falcao AFO, Gato LMC, Nunes EPAS. A Novel Radial Self-Rectifying Air Turbine for Use in Wave Energy Converters. Renewable Energy 2013;50:289–98.
[21] Falcao AFO, Gato LMC, Nunes EPAS. A Novel Radial Self-Rectifying Air Turbine for Use in Wave Energy Converters. Part2. Results from Model Testing. Renewable Energy 2013;53:159–64.
[22] Heller V, Chaplin JR, Farley FJM, Hann MR, Hearn GE. Physical Model Tests of the Anaconda Wave Energy Converter. In Proc. 1st IAHR European Congress, 2000.
[23] Vicinanza D, Frigaard P. Wave Pressure Acting on a Seawave Slot-Cone Generator. Coastal Engineering 2008;55(6):553–68.
[24] Fernandez H, Iglesias G, Carballo R, Castro A, Fraguela JA, Taveira-Pinto F, Sanchez M. The New Wave Energy Converter Wavecat: Concept and Laboratory Tests. Marine Sructures 2012;29(1):58–70.
[25] Dalton GJ, Alcorn R, Lewis T. Case Study Feasibility Analysis of the Pelamis Wave Energy Converter in Ireland, Portugal and North America. Renewable Energy 2010;35(2):443–55.
[26] Latosov E, Volkova A, Siirde A, Kurnitski J, Thalfeldt M. Methodological Approach to Determining the Effect of Parallel Energy Consumption on District Heating System. Environmental and Climate Technologies 2017;19(1):5–14.
[27] De B, Mukherjee M. Optimizing Street Canyon Orientation for Rajarhat Newtown, Kolkata, India. Environmental and Climate Technologies 2017;21(1):5–17.
[28] Hassan MT, Burek S, Asif M. Barriers to Industrial Energy Efficiency Improvement–Manufacturing SMEs of Pakistan. Energy Procedia 2017;113:135–42.
[29] Gorcun OF. Reduction of energy costs and traffic flow rate in urban logistics process. Energy Procedia 2017;113:82–9.
[30] Viba J, Beresnevich V, Irbe M, Dobelis J. The control of blades orientation to air flow in wind energetic device. Energy Procedia 2017;128:302–8.
[31] Jafari M, Sojoudi A, Hafezisefat P. Numerical Study of Aeroacoustic Sound on Performance of Bladeless Fan. Chinese Journal of Mechanical Engineering 2017;30(2):483–94.
[32] Jafari M, Afshin H, Farhanieh B, Bozorgasareh H. Numerical aerodynamic evaluation and noise investigation of a bladeless fan. Journal of Applied Fluid Mechanics 2015;8(1):133-42.
[33] Jafari M, Afshin H, Farhanieh B, Bozorgasareh H. Experimental and Numerical Investigation of a 60cm Diameter Bladeless Fan. Journal of Applied Fluid Mechanics 2016;9(2):935-944.
[34] Jafari M, Afshin H, Farhanieh B, Sojoudi A. Numerical investigation of geometric parameter effects on the aerodynamic performance of a Bladeless fan. Alexandria Engineering Journal 2016;55(1):223-33.
[35] Smith A. Patent Application Publication, US 2013/0052042 A1. Pumping Device.
[36] Bhinder M, Mingham C, Causon D, Rahmati M, Aggidis G, Chaplin R. Numerical and Experimental Study of a Surging Point Absorber Wave Energy Converter. In Proceedings of the 8th European wave and tidal energy conference, Sweden, Uppsala, 2009.
[37] Fox RW, McDonald AT, Pritchard PJ. Introduction to Fluid Mechanics. New York: John Wiley & Sons; 1985.
[38] Negahdari M, Baigzade B, Dalayeli H. Design of Mechanical Device to Convert Sea Wave Energy to Electrical Energy. In Proceedings of the national conference on sea water utilization. Iran, Kerman, 2012;445–55.
[39] Rusu E, Onea F. Evaluation of the wind and wave energy along the Caspian Sea. Energy 2013;50:1–4.